International Journal of Microwave and Wireless Technologies, 2011, 3(2), 201–211.
doi:10.1017/S1759078711000092

60 GHz short-range communications: channel measurements, analysis, and modeling

ALEXIS PAOLO GARCIA ARIZA[1], UWE TRAUTWEIN[2], ROBERT MÜLLER[1], FRANK WOLLENSCHLÄGER[1], REINER S. THOMÄ[1], JÜRGEN KUNISCH[3], ITZIAR DE LA TORRE[3], ROBERT FELBECKER[4], MICHAEL PETER[4] AND WILHELM KEUSGEN[4]

This article presents measurement and analysis results for 60 GHz short-range wideband radio channels. We consider two scenarios, referred to as "very-high-rate extended-range" (VHR-E) and "ultra-high-rate cordless" (UHR-C). The VHR-E measurements aimed at 60 GHz fixed networks for an Airbus A340 cabin both under static and dynamic (shadowing due to passenger movement) channel conditions. We describe the channel sounder used for the VHR-E measurements and present a simple multipath model derived from the measurements. Furthermore, simulations show the feasibility of the ray-tracing approach for this kind of channel. As a typical UHR-C use case, a data kiosk scenario was investigated. Various propagation conditions are analyzed with respect to channel gain, time dispersion, and frequency selectivity.

Keywords: 60 GHz Radio Channel, Millimeter-waves, Channel Measurements, Channel Sounding, Channel Modeling, Ray-Tracing, In-cabin Propagation, In-flight-Entertainment, Shadowing by Human Bodies, Uncompressed Video, Time-varying Channels, Wireless Channels, Data Kiosk, Fast Download, Ultra-high-rate, Cordless, Wideband

Received 15 November 2010; Revised 20 January 2011; first published online 22 March 2011

I. INTRODUCTION

The 60 GHz frequency band, which provides up to 9 GHz of unlicensed bandwidth, is a highly promising resource for future wireless short-range transmission. It is intended to be used for high-rate wireless networks (Wireless Local Area Network (WLANs), Wireless Personal Area Network (WPANs)) as well as for ultra-high rate point-to-point links, addressing applications like high-definition (HD) video streaming, wireless in-flight/in-car entertainment and ultra-high speed content download.

The German EASY-A project [1] has focused on early prototype transceiver implementations to demonstrate the capability of 60 GHz technology for specific applications. Since short-range multi-gigabit/s transmission heavily depends on the conditions of the underlying radio channel, application-specific channel investigations have been an essential issue within the project to derive design and link budget parameters and to provide the basis for detailed link-level simulations. Two scenarios, namely very-high-rate extended range (VHR-E) and ultra-high-rate cordless (UHR-C) are considered, which focus on different applications and physical layer implementations. Whereas VHR-E systems are intended to achieve up to 3 Gbit/s over a distance of 10 m, rates up to 10 Gbit/s over a distance of 1 m are targeted with UHR-C systems.

It is known from previous investigations that 60 GHz radio channels do not follow the usual 2–5 GHz characteristics [2], showing smaller delay spread [3] and remarkable dependence on human activity [4]. The latter aspect is especially important with respect to VHR-E systems, which are intended to be used in Public Transportation (PT) environments involving numerous users and intense human activity. On the other hand, intra-/inter-system interference and antenna alignment are also key issues in order to keep acceptable QoS levels for real-time applications and HD video streaming. Performance analysis of new MAC/PHY techniques, such as pixel-partitioning and multi-antenna-beam methods [5], requires real-time, full bandwidth channel sounding (7–9 GHz bandwidth), and multi-antenna capability if macro-diversity, seamless handover, or beamforming are considered for analysis.

Thus, in Section II a 60 GHz-UWB real-time multi-antenna channel sounder (RTMCS) is addressed along with its application to multi-gigabit/s deployment for VHR-E scenarios. The modular concept is introduced and channel analyses are presented for a PT environment. Based on a measurement campaign carried out within an Airbus 340 cabin, the achievable coverage, the coherence bandwidth, and the delay spread of the channel as well as the impact of shadowing are discussed. The evaluations involve different PHY channelizations, access point configurations (APCs), antennas, and human activities. Based on the channel measurements, a line-of-sight (LOS) single exponential decay cluster model is defined with a summary of the

[1]Ilmenau University of Technology, Institute of Information Technology, Helmholtzplatz 2, 98684 Ilmenau, Germany. Phone: +49-3677-691397.
[2]MEDAV GmbH, Gräfenberger Strasse 32-34, 91080 Uttenreuth, Germany.
[3]IMST GmbH, Carl-Friedrich-Gauss-Strasse 2-4, 47575 Kamp-Lintfort, Germany.
[4]Fraunhofer Heinrich Hertz Institute, 10587 Berlin, Germany.
Corresponding author:
A. P. Garcia Ariza
Email: alexis-paolo.garcia-ariza@tu-ilmenau.de

corresponding model parameters like multipath cluster envelope level, cluster decay coefficient, and correlation coefficient of the cluster envelope. Some comparative ray-tracing results are also given in this section to validate the possibility of simulating the wave propagation in this environment deterministically, which is important for further analysis of coverage and antenna configurations.

In contrast to the VHR-E scenario, the ultra-high-rate cordless (UHR-C) scenario relies on a channel that is mainly constituted by the direct propagation path (LOS path), thus Additive white Gaussian noise (AWGN) conditions may be assumed for coarse estimations of the link performance. However, with regard to data rates up to 10 Gbit/s in combination with the aim to use low complexity transceiver implementations, channel characterization accounting for even small multipath effects is necessary to allow reliable predictions on the system performance. An extensive channel measurement campaign with focus on a data kiosk scenario, as a typical use case for UHR-C, has been carried out in order to analyze the time dispersion and the frequency selectivity of highly LOS-dominated 60 GHz channels. Different configurations and propagation conditions have been considered to investigate the dependence of the channel on transmission distance, alignment errors, polarization, and people in close vicinity to the LOS. Section III briefly describes the data kiosk scenario as focused application for UHR-C and presents selected results of the aforementioned measurement campaign.

II. VHR-E SCENARIO

A) In-cabin environment

As VHR-E systems are intended to be used in PT environments involving numerous users and intense human activity, a measurement campaign for a VHR-E scenario in static and dynamic conditions has been carried out in an Airbus 340 mockup. This indoor PT environment is located at the European Aeronautic Defence and Space Company – (EADS), Innovation Works; see Fig. 1. It is 6.4 m long and 5.6 m wide and comprises four chair rows and two aisles of 0.6 m width. Two APCs (scenarios 1 and 2) have been considered for testing different access point (AP, these were the receivers (Rxs) during the measurement campaign) locations and dynamics due to human activity (see Fig. 1 right) with passengers walking through the aisles and the seat rows. APC1 provides APs close to the cabin windows, whereas for APC2 the APs are located in the middle of the cabin. AP1 is located in the front of the mockup and AP2 in the back. Figure 1 left illustrates the transmitter (Tx) positions, which represent the seat-tag terminals of e.g. in-flight-entertainment (IFE) systems.

We considered antennas with different beamwidths (see Fig. 2) for the campaigns. For the in-cabin coverage analysis, two commercial antennas have been used, i.e., an open-ended waveguide (OWG) WR15 with about 8 dBi and 42° (*E*-plane) half-power beamwidth (HPBW), and a horn (HORN) antenna with about 22.6 dBi and 12° HPBW (*E*-plane). Other antennas, designed on low-temperature co-fired ceramics (LTCC) have been included in the analysis of shadowing by human bodies (SHB). These are a 2×2 patch array (PATCH) with 8.2 dBi and 36° HPBW (*E*-plane) [6], and a 2×1 cavity array (CAV) with 8.6 dBi and 62° HPBW (*E*-plane) [7]. A commercial omnidirectional (OMNI) antenna (in *H*-plane) with 0.7 dBi with 102° HPBW (*E*-plane) has been included in Fig. 2 as reference. It is worth mentioning that antennas with higher directivity reduce the temporal dispersion in indoor environments but increase both the fading margins due to SHB [4] and the losses due to misalignment. These are relevant characteristics for the 60 GHz link budget.

The different antenna beamwidths allowed us to perform a coverage analysis with different alignment at each seat row (according to the distance to the APs), as indicated in Fig. 1 left. The AP positions (these were the Rxs during the measurements) intended to cover all seat rows with a constant tilt of −10°. For reliable coverage comparisons between APs, the Tx antennas (representing seat-tag-terminal positions) were always pointing up to the ceiling using OWG due to its symmetric pattern. Note that CAV and PATCH antennas were not included for the coverage analysis. They were included for dynamic analysis instead, along with OWG and HORN.

The coverage measurements included different antenna combinations based on four APs, covering about five seats each. Thus, wide and narrow patterns were included at the APs (Rx's), and wide patterns at the Tx, i.e. $\mathrm{HORN_{RX1}}$–$\mathrm{OWG_{TX}}$–$\mathrm{HORN_{RX2}}$ and $\mathrm{OWG_{RX1}}$–$\mathrm{OWG_{TX}}$–$\mathrm{OWG_{RX2}}$ in horizontal polarization. For this measurement campaign, all Tx positions were distributed symmetrically through half of the cabin area. Besides, for measurements at each seat row and aisles, a robotic positioning system was implemented (with 5 cm resolution along 2.5 m). More details about the system configuration can be found in [3, 4].

The 60 GHz up-converter implemented for channel sounding allowed ∼15 dB of conversion gain. Hence, ∼15 dBm transmit power at the 60 GHz stage is gained for an IF input of 0 dBm at the UWB stage. Therefore, equivalent isotropically radiated power between 15 and 37 dBm has been considered for each AP. The 60 GHz up-/down-converters covered the lower wideband channel (2.16 GHz bandwidth) of the 60 GHz WLAN/WPAN channel plan [8], and 0.94 GHz of the consecutive channel. The used channel plan alternatives have been included for coverage analysis in the described VHR-E scenario.

B) Measurements

A novel 60 GHz-UWB real-time channel sounder architecture has been implemented at Ilmenau University of Technology in cooperation with MEDAV GmbH [3] (see Fig. 3), which has been used for the measurement campaigns in the cabin mockup. This channel sounder is based on an UWB sounder architecture [9] and a stage of frequency conversion from/to the UWB band (3.5–10.5 GHz) to/from the 60 GHz band (59.5–66.5 GHz). Multiple-input–multiple-output capability is supported by using multiple modules. This concept allowed us to study the channel dynamics due to SHB and for the first time its auto-correlation and cross-correlation characteristics for macro-diversity and handover implementations [4]. Besides, this sounder solution allows channel parameter extraction for realistic system simulations at PHY and MAC levels. This means that performance analysis during long-time data transmissions including statistics due to human events can be performed. Moreover, this 60 GHz-UWB RTMCS permits us to carry out indoor radio network planning for VHR-E scenarios, e.g., for deployment of IFE systems. This sounder architecture covers most of the

https://doi.org/10.1017/S1759078711000092 Published online by Cambridge University Press

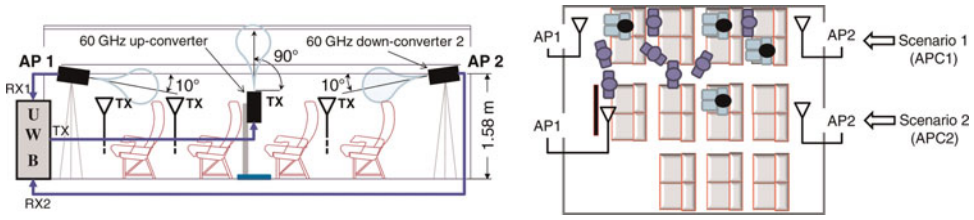

Fig. 1. Schematic of the A340 mockup at EADS-IW with APs and Tx relative positions: side view (left) and top view (right).

assigned 60 GHz spectrum around the world, so facilitates analyzing data (in post-processing) at four different sub-bands as established at the IEEE 802.15.3c PHY channelization, i.e., from 59.40 to 61.56 GHz, from 61.56 to 63.72 GHz, and from 63.72 to 65.88 GHz. Different narrow and wideband channel plans can also be analyzed with this architecture for the IEEE 802.11.ad standard [8].

The performance of our first sounder implementation with 3 GHz bandwidth (from 59.5 to 62.5 GHz), real-time single-input–multiple-output (SIMO) capability (one Tx and two Rx), and linear polarization (horizontal at APs during measurements) has been verified. Once the calibration was performed and the frequency span set (in post-processing from 59.5 to 62.5 GHz, to avoid noisy bins from the full 7 GHz bandwidth), the dynamic range of the system reaches up to approximately 50 dB. This results in an experimental resolution of ∼1 ns (maximum 0.333 ns) with maximum detectable paths up to ∼585 ns [10]. These sounding

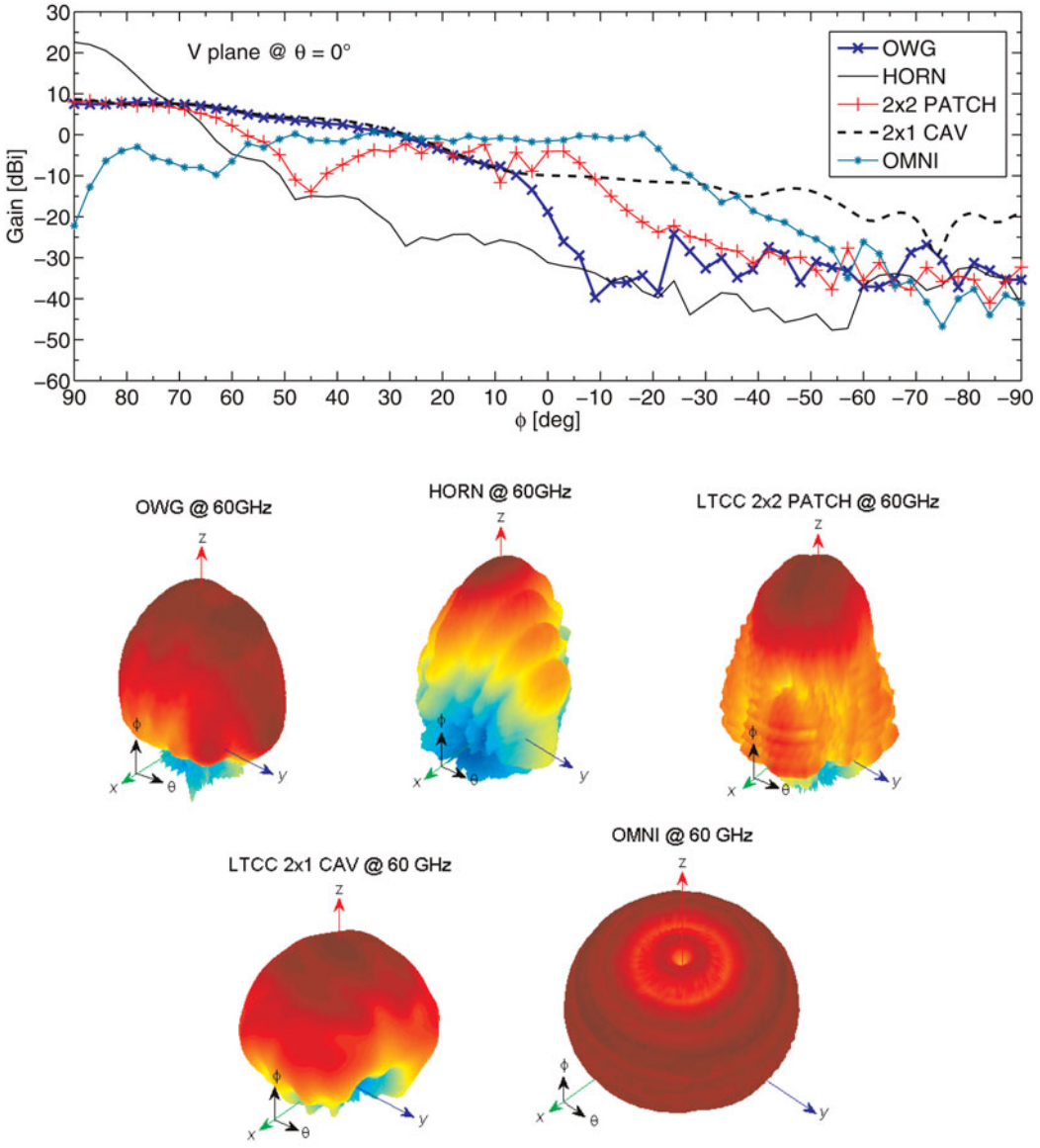

Fig. 2. Measured antenna patterns at 60 GHz for commercial and EASY-A antenna arrays on LTCC: V planes (top) and shapes of the antenna patterns (bottom).

https://doi.org/10.1017/S1759078711000092 Published online by Cambridge University Press

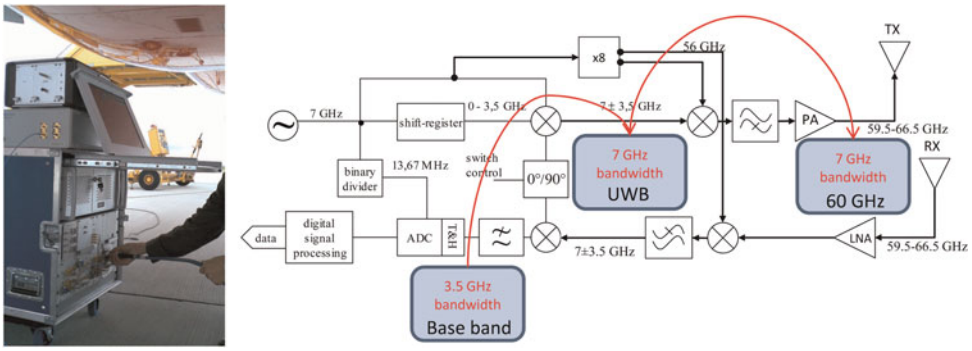

Fig. 3. Channel sounder architecture for 60 GHz-UWB time-varying channel measurements: UWB channel sounder (left) and 60 GHz-UWB architecture (right).

characteristics guarantee enough dynamic range for SHB analysis and the best sounding resolution reported in literature based on a real-time SIMO configuration at 60 GHz. It is worth mentioning that new sounder implementations include dual-polarized frontends with 7 GHz bandwidth in real time with digital/analog phase control [11]. This 60 GHz-UWB RTMCS will allow us to perform full channel characterization including polarization mismatch, alignment, and estimation of direction of arrival and direction of departure based on synthetic aperture measurements.

C) Analysis

1) COVERAGE

The goal was to perform an outage analysis (from cumulative distributions) depending on AP coverage. For each Tx location, using 10 snapshots (average), the SNR was calculated using the ratio from the channel impulse response power to the theoretical noise power. Table 1 shows the SNR results in the cabin coverage area for OWG and HORN (averaging APC1 and APC2; Rxs are OWG or HORN, respectively; Tx was always an OWG) for two different bandwidths (lower channel from the 60 GHz WLAN/WPAN channel plan and full channel sounder bandwidth). It has been found that HORN offers better SNR results at high outage values. At 90% outage, HORN offers about 4 and 3.5 dB more than OWG for 2.16 and 3 GHz bandwidth, respectively. However, for 10% outage (guarantying a certain SNR level for 90% of locations) both antenna patterns offer similar performance. Note that at median values (50% outage) HORN offers about 2 dB more than OWG for both bandwidths.

The lower sub-band (59.40–61.56 GHz) offers the best performance for system deployment in the current scenario, getting even better using HORN. But under these conditions, only 10% of the in-cabin analyzed area (see results at 90% outage) offers enough power for a reliable Quadrature Phase Shift Keying (QPSK) modulation/demodulation with SNR requirements greater than 10 dB, being feasible a target bit rate of 2 Gbit/s for approximately 2 seats per AP. Note that these results have been obtained with the Tx pointing to the ceiling and for independent APs. This indicates that alignment of antennas is mandatory for reaching better coverage, and handover between APs should be considered for improving the reliability of the system.

On the other hand, 50% of the coverage area offers an SNR of about 6 dB for OWG, and around 8 dB for HORN, using the lower sub-band of the IEEE 802.15.3c channel plan. This means that a low-power mode with a lower bit rate can be considered for at least 10 seats. To increase the coverage area, the down link could also be switched to a more robust modulation scheme with a compressed video mode. For 10% outage, all possible configurations and bandwidths did not offer enough SNR. This happened mainly due to the low receiver power for the seat-tag locations located below APs, which could be served by other APs in an in-cabin cellular configuration.

Note that for 3 GHz bandwidth, a lower SNR is a consequence of many factors: higher noise power in the full bandwidth, higher frequency components, and antenna gain reduction versus frequency. Differences on the SNR distributions between the analyzed sub-bands and an upper band of 0.94 GHz have been considered in [10].

Table 1. SNR coverage – outage results for the A340 mockup.

Bandwidth (GHz)	% Outage→ $OWG_{APs}/HORN_{APs}$		
	90%	**50%**	**10%**
2.16	11.41/15.26 dB	6.44/8.24 dB	1.14/1.82 dB
3	7.35/10.93 dB	2.29/4.35 dB	o/o dB

2) IN-CABIN STATIC CHANNEL

Outage results of the root-mean-square delay spread, τ_{rms} for 10, 20, and 30 dB thresholds, and coherence bandwidth at 0.9 in the frequency auto-correlation, $B_{coh,o.9}$, are presented in Table 2 (using 3 GHz bandwidth in all cases). The main conclusion is that the delay spread $<$10.16 ns at 90% outage (and $<$15 ns for higher outage values [10]) considering all Tx locations for every possible configuration and antenna, even at 30 dB threshold. However, using HORN at the Rx, higher time dispersion was obtained at 90% outage compared with OWG. Taking into account the antenna HPBWs from Fig. 2, these results are a consequence of the wide coverage area with low power due to the high directionality of the HORN antennas (most of the Tx positions were in misalignment). However, at 10% outage HORN depicts lower delay spreads than OWG, which is caused by a small group of Tx locations in better alignment and close to the APs (about two seats in each APC). This behavior is also reflected in the $B_{coh,o.9}$ results. OWG depicts higher values than HORN at 90% outage, reaching up to 400 MHz in some locations. At 50% outage, the $B_{coh,o.9}$ is always (for both APs and APCs) lower than 10 MHz, and HORN reaches higher values than OWG, even at 10% outage. Finally, note that Table 2 was obtained from distributions considering all of

https://doi.org/10.1017/S1759078711000092 Published online by Cambridge University Press

Table 2. Delay spread and coherence bandwidth – outage results for the A340 mockup.

		% Outage					
		90%		50%		10%	
		OWG	HORN	OWG	HORN	OWG	HORN
τ_{rms} (ns)	10 dB	4.19	6.6	1.42	1.37	0.19	0.16
	20 dB	6.42	8.79	4.52	5.34	2.4	1.18
	30 dB	7.37	10.16	5.91	6.95	3.95	2.87
$B_{coh,0.9}$ (MHz)		30	16.6	7.8	9.57	~5	~7

the locations along the cabin. Thus, these % outage results are related to the whole coverage area for both AP and APCs, not to local areas, i.e. these results correspond to statistics for large-scale analysis.

3) IN-CABIN DYNAMIC CHANNEL

Here the analysis is focused on the dynamics of the channel due to human activity based on the SHB parameters (mainly fading due to obstruction of LOS) as indicated in [4]. HORN, OWG, PATCH, and CAV have been included for SHB analysis as possible antennas to be implemented during deployment of an IFE system, with special interest on LTCC antennas due to their small size and easy packaging for mass production. Table 3 includes the experimental results of SHB for in-cabin planning purposes of 60 GHz WLAN/WPAN. Instead of using outage results, we present reliability results for fading margins in dB (needed for link budgets). Thus, the worst case was found for the antenna combination CAV_{APs}–CAV_{TX}, depicting SHB margins of 22.3 dB at 99% reliability. The best case using LTCC antennas was found with CAV_{APs}–$PATCH_{TX}$, with 11.7 dB at 99% reliability. For usual commercial antennas (as used in the SNR analysis of Table 1), the worst cases were found for $HORN_{APs}$–OWG_{TX}, with SHB margins of 17 dB at 99% reliability. Note that median values (indicated as 50%) remain around ~2 to ~4 dB for different antenna combinations, except for CAV_{APs}–CAV_{TX}. For 90% reliability all fading margins were reduced with a remarkable drop using HORN at the APs. Hence, according to the possible link budget constraints and QoS requirements for an IFE system, fading margins at 90% reliability could be a suitable choice for increasing the in-cabin coverage area. Nevertheless, note that these margins are much larger than usual values obtained at lower frequencies.

Distribution results of SHB parameters for different antenna combinations are presented in [4], where SHB fading rates of about $\pm$10 dB/100 ms were observed. Thus, the experimental SHB margins and fading rates indicate that efficient techniques must be implemented to keep the receiver power within prescribed limits to fulfil the SNR targets, while providing fast buffer capabilities for PT scenarios. Besides, in case of LTCC antennas, the combination of wide- (62° HPBW) and medium-wide (36° HPBW) antenna patterns (see respectively CAV and PATCH in Fig. 2, and results in Table 3), compared with the CAV_{APs}–CAV_{TX} solution, offers a useful solution for point-to-multipoint PT networks reducing fading margins due to human activity. Thus, this LTCC compact solution could be targeted for realistic implementations. For further 60 GHz enhancement techniques as macro-diversity or seamless handover, we have also studied the SHB auto-correlation and cross-correlation characteristics between APs using LTCC antennas, which are not addressed here but some results were presented in [4].

Table 3. Margins (in dB) of SHB – reliability results for the A340 mockup.

Antennas	Reliability		
	50%	90%	99%
OWG_{APs}–OWG_{TX}	2.5	7.6	8.8
$HORN_{APs}$–OWG_{TX}	4.1	7.1	17
CAV_{APs}–$PATCH_{TX}$	2.3	8.2	11.7
CAV_{APs}–CAV_{TX}	10	19.9	22.3

D) Modeling

1) IN-CABIN STATISTICAL MULTIPATH MODEL

a) Power delay profiles

Figure 4 shows examples for power delay profiles determined from the coverage measurements. The power delay profiles are normalized to the measurement bandwidth B; consequently, the level of a single isolated path (e.g. the direct path) corresponds to the path gain (e.g., a direct path level of −85 dB corresponds to −85 dB path gain). In all plots, a Kaiser–Bessel ($\alpha = 2.0$) frequency domain window has been used. In all cases the power delay profiles exhibit, as a first approximation, a single exponential decay cluster plus a more or less pronounced dominant (direct) path, plus occasional isolated paths. The clusters decay below the measurement noise level at no more than approximately 100 ns. Note that in several cases (e.g. left plot in Fig. 4), the multipath envelope exhibits an initial onset region as has been observed for certain other (e.g. indoor and industrial) UWB channels (cf. [12, 13]).

b) LOS plus single exponential decay cluster model

Based on the power delay profile properties discussed above, a simple multipath model for the unobstructed coverage measurements consists of a LOS path (to be determined from geometry and antenna patterns), augmented by a single exponential decay cluster (as defined in the Saleh–Valenzuela model [14]).

The multipath cluster envelope is given by $|h(\tau)^2| \sim \exp(-\tau/\gamma)$, where $h(\tau)$ is the impulse response, γ is the cluster decay coefficient, and τ is the time delay. In this simple model, the ray arrival is assumed to follow a homogeneous Poisson process with arrival rate $\lambda = B$. The power of the multipath cluster is characterized by the power Δ of the model cluster envelope at the LOS delay, given in dB with respect to the LOS power. The corresponding model parameters are summarized in Table 4.

Note that due to the onset region described above this model tends to overestimate early multipath components.

https://doi.org/10.1017/S1759078711000092 Published online by Cambridge University Press

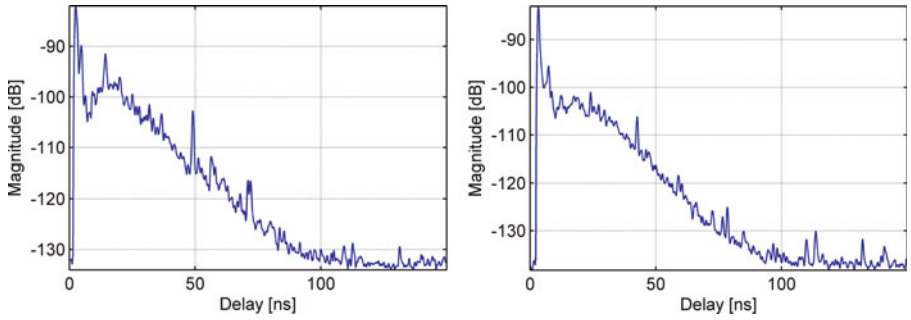

Fig. 4. Example power delay profiles (coverage measurements).

Table 4. Single-cluster model parameter description.

Parameter	Description
Δ	The multipath cluster envelope level at the LOS delay given in dB with respect to the LOS path level
γ	The cluster decay coefficient
ρ	The correlation coefficient of the cluster envelope magnitude (in dB) as function of delay ($\rho = -1$ corresponds to a straight line, i.e. an ideal exponential decay envelope)

Table 5 summarizes the mean values and standard deviations of the model parameters for several data subsets corresponding to various combinations of measurement parameters. In the table, an overbar and the symbol σ indicate average and standard deviation, respectively. Furthermore, an asterisk (*) indicates any possible value. For example, the last line in Table 5 corresponds to the entire dataset and shows that the overall cluster decay coefficient average is in the order of $\gamma = 8$ ns, with a standard deviation of less than 1 ns, whereas the average cluster power equals approximately -7 dB (with respect to the LOS power), with a 2.5 dB standard deviation.

Table 5. Single-cluster model parameter values.

AP antenna	APC	AP	$\bar{\Delta}$	σ_Δ	$\bar{\gamma}$	σ_γ	$\bar{\rho}$	σ_ρ
			dB	dB	ns	ns		
HORN	APC1	AP1	−7.8	2.1	8.3	0.9	−0.9819	0.0053
HORN	APC1	AP2	−9.0	2.6	8.8	0.6	−0.9839	0.0048
HORN	APC2	AP1	−5.1	0.0	8.7	0.0	−0.9825	0.0000
HORN	APC2	AP2	−7.0	1.4	9.2	0.8	−0.9868	0.0052
OWG	APC1	AP1	−5.7	2.9	7.4	0.3	−0.9946	0.0013
OWG	APC1	AP2	−6.4	3.1	7.4	0.1	−0.9923	0.0090
OWG	APC2	AP1	−7.3	2.0	7.2	0.1	−0.9958	0.0009
OWG	APC2	AP2	−7.1	1.2	7.5	0.0	−0.9961	0.0007
HORN	APC1	*	−8.3	2.3	8.5	0.8	−0.9828	0.0049
HORN	APC2	*	−6.5	1.5	9.1	0.7	−0.9858	0.0048
OWG	APC1	*	−6.1	2.9	7.4	0.2	−0.9934	0.0062
OWG	APC2	*	−7.2	1.5	7.3	0.1	−0.9960	0.0008
HORN	*	AP1	−7.4	2.1	8.4	0.8	−0.9820	0.0048
HORN	*	AP2	−8.2	2.4	8.9	0.6	−0.9850	0.0048
OWG	*	AP1	−6.2	2.6	7.4	0.3	−0.9950	0.0013
OWG	*	AP2	−6.7	2.5	7.4	0.1	−0.9936	0.0074
HORN	*	*	−7.8	2.2	8.7	0.8	−0.9836	0.0049
OWG	*	*	−6.4	2.5	7.4	0.2	−0.9943	0.0052
*	APC1	AP1	−6.7	2.6	7.9	0.8	−0.9883	0.0076
*	APC1	AP2	−7.6	3.0	8.0	0.8	−0.9884	0.0083
*	APC2	AP1	−6.7	2.0	7.6	0.7	−0.9925	0.0067
*	APC2	AP2	−7.0	1.2	8.3	1.1	−0.9915	0.0061
*	APC1	*	−7.2	2.8	7.9	0.8	−0.9883	0.0077
*	APC2	*	−6.9	1.4	8.0	1.0	−0.9919	0.0060
*	*	AP1	−6.7	2.4	7.8	0.8	−0.9893	0.0074
*	*	AP2	−7.4	2.5	8.1	0.9	−0.9895	0.0075
*	*	*	−7.1	2.5	8.0	0.8	−0.9894	0.0074

2) IN-CABIN RAY-TRACING MODEL

Several ray-tracing simulations (based on the tool "Wireless Insite" from Remcom [15]) were performed for comparison with the results from the measurement campaigns carried out at the A340 mockup (cf. Fig. 1). For this, a 3D simulation model of the mockup was built (see Fig. 5) using relatively few objects (534 faces). The achieved accuracy underlines the feasibility of low-resolution modeling, which also leads to drastically reduced computation times.

On basis of the setup in the measurement campaigns, the parameters for the Tx and Rx were selected, including the antenna diagrams and their orientation. The electrical properties of the involved materials were taken from [16]. The total number of allowed interactions was set to six reflections and four transmissions. Figure 6 shows an example of the magnitude of 51 channel impulse responses obtained along a Tx rail line in 5 cm steps.

An instance of a comparison between simulated and measured power delay profiles is presented in Fig. 7, where the power delay profiles were estimated by taking the root-mean-square average of the 51 impulse responses along the Tx rail line. A considerable result is that the slope of the exponential cluster decay in the simulations is comparable to the measurements. Nevertheless, it is worth to mention that there are some differences between both curves. Particularly, there are some effects in the measurements that are not reproducible in the simulations, but mostly all the important features are recognizable, although the magnitude does not match exactly in all cases. Note that the electric

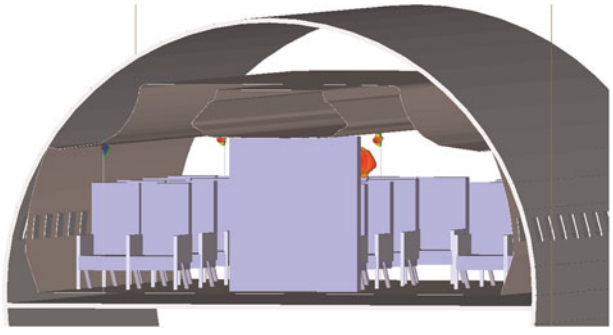

Fig. 5. 3D Model used for ray tracing (front view).

https://doi.org/10.1017/S1759078711000092 Published online by Cambridge University Press

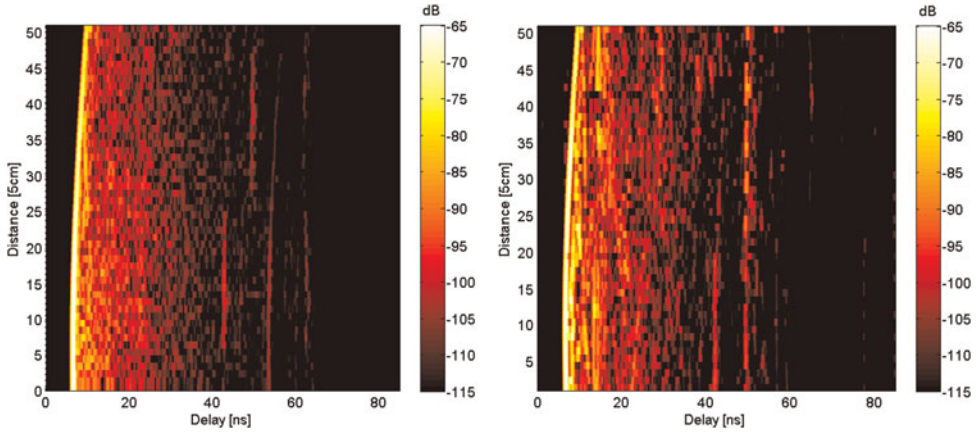

Fig. 6. Normalized channel impulse response magnitude along a Tx rail line: (a) measurement and (b) simulation.

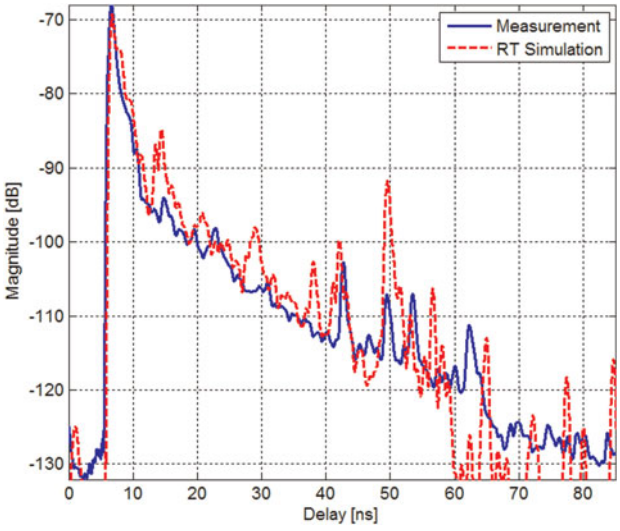

Fig. 7. Comparison between measured and simulated power delay profiles.

properties of the materials, the definition of the 3D model, and the accuracy of the antenna patterns have a notable influence on the simulated results.

Further ray-tracing results (focusing on the optimization of access-point and seat-tag configurations for a typical European single aisle aircraft cabin) can be found in [17].

III. UHR-C SCENARIO

A) Data kiosk transmission

Ultra-high speed data download from a data kiosk is the focus of the UHR-C scenario. Data rates of 10 Gbit/s are considered for distances up to 1 m in quasi-static conditions. In order to model the transmission scenario, a set-up was built, which allows measuring the channel for different transmission distances, as shown in Fig 8. Figure 9 illustrates the configuration with a user and a disturbing person near the data kiosk. The user is assumed to point a handheld device towards the kiosk to download a large amount of data.

Several factors have to be taken into account with respect to the kiosk scenario. The main problem is misalignment of the handheld. Another issue is related to possible disturbances by

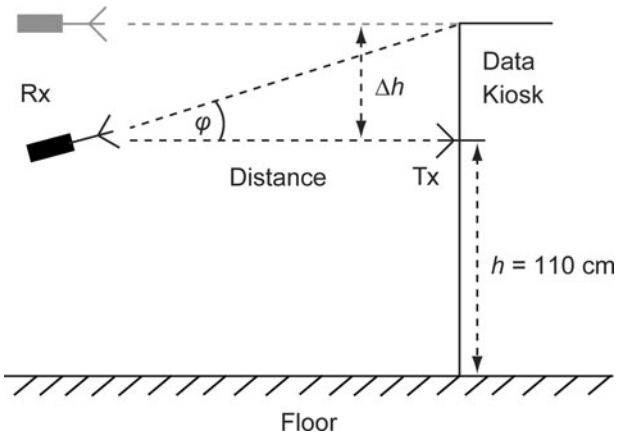

Fig. 8. Measurement configuration for the data kiosk scenario.

other persons during the data transfer. To cover these factors, measurements were carried out for two distances between handheld and data kiosk (50 and 100 cm) including

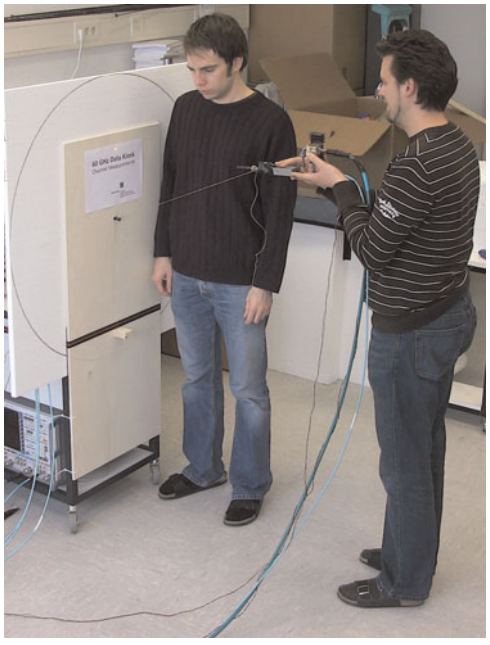

Fig. 9. Data kiosk scenario with user and disturbing person.

https://doi.org/10.1017/S1759078711000092 Published online by Cambridge University Press

misalignment and people standing in close vicinity to the LOS. The basic measurement arrangement for the measurements with misaligned Rx is shown in Fig. 8, where we distinguish between two practical types of misalignment: a height/lateral offset Δh and an angular misalignment ϕ. The maximum offset was ± 25 and ± 50 cm for 50 and 100 cm distance, respectively. The angular mismatch was kept below $\pm 27^\circ$ in both cases. The gathered dataset comprises 1600 frequency responses for statistical evaluations and simulation purposes.

Another configuration with the Rx fixed to an adjustable wooden rail was used to measure the channel over a distance from 10 to 100 cm in 5 cm steps. These results served as a basis to derive path loss parameters.

B) Measurement equipment

An R&S ZVA24 vector network analyzer and a frequency extension setup were used to capture the channel in the frequency range from 50 to 72 GHz with a step width of 4 MHz. In the time domain, this results in a multipath resolution of approximately 45.5 ps. OWGs with a gain of approximately 8 dBi served as transmit and receive antennas.

C) Measurement results

1) CHANNEL GAIN AND PATH LOSS

In contrast to typical 60 GHz indoor channels with distinct multipath components as analyzed in Section II and in [18, 19], the 60 GHz data kiosk channel is dominated by the LOS component (see Fig. 10). Nevertheless, several weak clusters of multipath components show up in the averaged power delay profiles (APDPs), which are obtained by averaging over 100 individual power delay profiles. Due to the arrangement of the measurement setup the multipaths can be attributed to a ground reflection, a reflection from the ceiling and reflections from the surrounding walls. Figure 10 shows the APDPs arising for vertical (VV) and horizontal (HH) polarization at 100 cm distance. It can be observed that the first multipath components, which result from reflections from the floor and the ceiling, are slightly stronger for vertical polarization. In principle, higher reflection losses would be expected in this case due to the parallel orientation of the electric field vector with respect to the plane of reflection. However, for the occurring reflection angles, the reflection loss is nearly equal for both polarizations. Furthermore, the reflections for vertical polarization benefit from the radiation pattern of the OWG, which is less directional in the *E*-plane than in the *H*-plane of the antenna.

Regarding misalignment, the measurement results reveal moderate variations around ± 4 dB of the channel gain (C_G, ratio of average received signal power to average transmit power) regardless of the polarization. In principle, polarization multiplexing (vertical, horizontal) can be utilized to maximize the spectral efficiency in LOS environments. However, it is a suitable method only when polarization crosstalk remains below a certain limit. In order to assess the crosstalk, C_G has not only been derived from co-polar (CO) but also from cross-polar (CR) antenna arrangements. The cumulative distributions for 50 and 100 cm are illustrated in Fig. 11. Note that the variation of the channel gain for the CR antenna configuration is higher than for co-polarized antennas since small deviations from ideal orientation have a much stronger impact in this case. The most important information that can be taken from Fig. 11 is that the distance of the CO and the corresponding CR curves is between 10 and 30 dB (about 20 dB at the median values). These results indicate that polarization multiplexing might be deployed beneficially in connection with robust transmission schemes in many cases. However, crosstalk of this type can lead to unacceptable error floors for practical implementations [20] as long no mechanisms are applied that are capable to adapt the transmission to the instantaneous crosstalk conditions.

The path loss measurements yield a path loss exponent of 1.97 and an intercept point of 49.07 dB with respect to 10 cm reference distance. Expectably, these results are practically identical to values for free space propagation.

2) TIME DISPERSION AND FREQUENCY SELECTIVITY

The root-mean-square delay spread τ_{rms} (we used a threshold of -40 dB relative to the strongest path.) and the coherence bandwidth (B_{coh}) as introduced in [18] are common measures for time dispersion and frequency selectivity of radio channels. At first sight, there does not seem to be a need to address these parameters for the kiosk scenario due to the distinct LOS character of the channel. However, it is important to keep in mind that data rates up to 10 Gbit/s are focused for UHR-C applications in combination with low-complexity transceiver concepts that might not make use of an equalizer

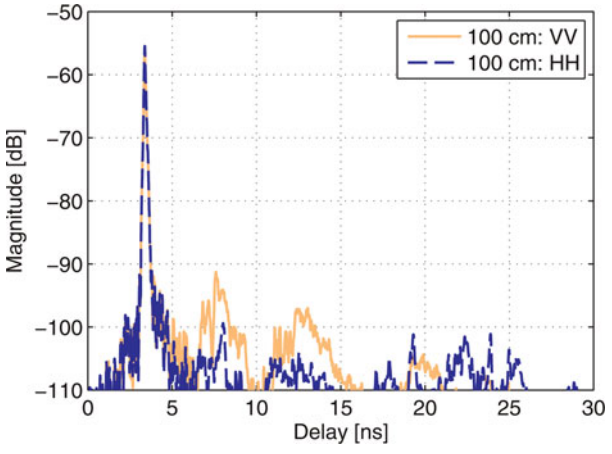

Fig. 10. APDP for a distance of 100 cm, and vertical (VV) and horizontal (HH) polarization of antennas.

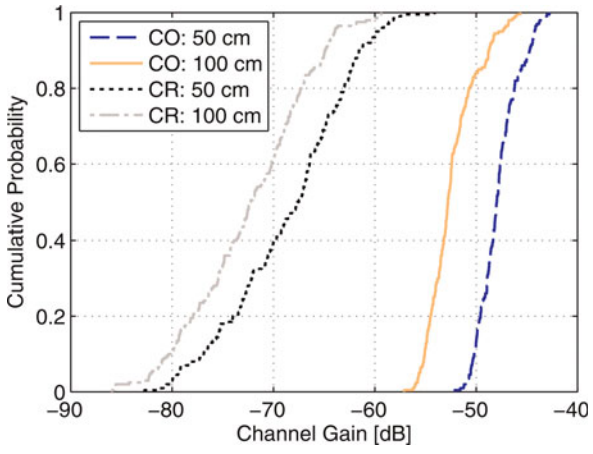

Fig. 11. Cumulative probability of the channel gain.

https://doi.org/10.1017/S1759078711000092 Published online by Cambridge University Press

Table 6. UHR-C channel parameters.

Parameter	Unit	Distance 50 cm				Distance 100 cm			
		HH	VV	HV	VH	HH	VV	HV	VH
$C_{G,min}$	dB	−52.1	−50.9	−81.5	−82.7	−57.1	−55.8	−82.3	−85.9
$C_{G,av}$	dB	−48.3	−47.3	−67.9	−69.2	−52.4	−52.4	−72.0	−72.7
$C_{G,max}$	dB	−43.0	−42.8	−54.1	−58.1	−45.7	−46.0	−59.4	−59.7
$\tau_{rms,min}$	ns	0.02	0.02	–	–	0.02	0.14	–	–
$\tau_{rms,av}$	ns	0.08	0.08	–	–	0.42	0.41	–	–
$\tau_{rms,max}$	ns	0.55	0.34	–	–	1.33	1.12	–	–
$B_{coh,0.9,min}$	GHz	1.31	1.36	–	–	1.30	1.29	–	–
$B_{coh,0.9,av}$	GHz	1.41	1.42	–	–	1.49	1.46	–	–
$B_{coh,0.9,max}$	GHz	1.54	1.50	–	–	1.69	1.67	–	–
$B_{coh,0.5,min}$	GHz	4.04	4.26	–	–	4.10	4.36	–	–
$B_{coh,0.5,av}$	GHz	4.58	4.61	–	–	4.93	4.81	–	–
$B_{coh,0.5,max}$	GHz	5.26	5.00	–	–	5.76	5.78	–	–

[20]. Hence, even delay spreads in the sub-ns region may cause serious intersymbol interference. A summary of the channel parameter values is given in Table 6.

First of all we observe maximum values of more than 1 ns for the delay spread at a distance of 100 cm between Tx and Rx and an increasing $\tau_{rms,av}$ with increasing distance. There is no significant change in τ_{rms} for the different polarizations, which can be explained by the different characteristics of the APDPs. In case of vertical polarization the early multipath components influence τ_{rms} significantly, while it is determined mostly by the later multipath components in case of horizontal polarization.

The coherence bandwidth, which has been calculated for correlation levels 0.9 and 0.5 of the frequency auto-correlation function, shows only slight dependencies on the distance and similar to the delay spread nearly no changes with respect to the different polarizations. Although the values in Table 6 give the impression of an irregular relation between coherence bandwidth and delay spread (both tendentially increase with distance), it has to be mentioned that we did not observe a general relationship between τ_{rms} and B_{coh} from one channel realization to another.

In [21] an analog-oriented transceiver concept is presented together with simulation results for QPSK modulation at a symbol rate of 3.5 GHz. AWGN as well as measured channels from this campaign have been considered. The results show that a reliable data transmission is possible even with channel distortions, although a performance loss up to approximately 1.5 dB can be observed with regard to a BER of 10^{-3}. This observation complies well with the values of $B_{coh,0.5}$, indicating that a symbol rate of roughly 4 GHz can be supported without equalization. However, intersymbol interference becomes a limiting factor if the rate is further increased.

Note that the channel measurements have also been performed in the presence of persons near the Tx without obstructing the LOS. Although their presence introduced some more multipath components, their impact on the channel gain, the delay spread and the coherence bandwidth was negligible.

IV. CONCLUSION

A real-time 60 GHz-UWB multi-antenna channel sounder has been implemented to perform channel measurements for a VHR-E scenario covering the IEEE 802.11ad and 802.15.3c channel plans. The subsequent measurement campaign has been carried out in an A340 mockup cabin as an example of a PT scenario. SNR coverage analysis, based on the measured results, indicated that alignment should be considered since only 10% of the coverage area reached SNR values high enough to guarantee at least 2 Gbit/s access. However, larger coverage areas with lower data rate access can be reached under low-power transmission modes. Concerning time dispersion and frequency selectivity, delay spread values always lower than 15 ns can be reported, whereas the median coherence bandwidth (at 0.9 correlation) was between ∼8 to ∼10 MHz for all configurations, antenna patterns, and Tx locations. These values are much smaller than the channel bandwidth available for the current wideband channel plans in IEEE 802.11ad and 802.15.3c. On the other hand, remarkable impact of human activity has been verified, which resulted in fading margins between 8.8 and 22.3 dB for 99% reliability using different antenna patterns. These channel results indicate that reliability enhancements of 60 GHz systems, including power constraints in link budgets for PT scenarios, can be reached with a proper antenna selection, or by applying macro-diversity, seamless handover, or beamforming. In this way, the potential of combining different small compact LTCC antennas for reducing SHB fading margins has been verified.

Relying on the channel measurement results and the Saleh–Valenzuela model, a statistical multipath model has been developed, including the common model parameters like multipath cluster envelope level, cluster decay coefficient, and correlation coefficient of the cluster envelope. Furthermore, ray-tracing simulation results of the 60 GHz channel using a 3D model of the A340 mockup have been compared with the measured data and showed a good match between simulations and measurements. Therefore, further channel analysis, regarding coverage and different antenna configurations using either the statistical multipath model or the 3D model and ray-tracing simulations will deliver valid results.

Apart from the channel analysis of the VHR-E scenario, an extensive channel measurement campaign for an UHR-C scenario has been carried out under various channel conditions. Misalignment of the handheld device, polarization crosstalk, and interference due to the presence of persons (besides the user) have been considered. The measurement results reveal only slight deviations from an AWGN channel and indicate that polarization multiplexing may be beneficially deployed. The presence of persons disturbing the transmission, although

https://doi.org/10.1017/S1759078711000092 Published online by Cambridge University Press

not obstructing the LOS, was found to have no significant influence on channel gain, time dispersion, and frequency selectivity. But on the other hand, values for the coherence bandwidth were observed to be very close to the bandwidth needed for the targeted symbol rate, which is in the range of several GS/s. This is most likely to become the critical issue when developing UHR-C systems without equalization.

ACKNOWLEDGEMENTS

This work was funded partly by the Federal Ministry of Education and Research of Germany (BMBF), within the "EASY-A: Enablers for Ambient Services & Systems, Part A – 60 GHz Broadband" (http://www.easy-a.de/) project.

REFERENCES

[1] Website: http://www.easy-a.de.

[2] Yang, H.; Smulders, P.F.M.; Herben, M.H.A.J.: Indoor channel measurements and analysis in the frequency bands 2 GHz and 60 GHz, in IEEE 16th Int. Symp. on Personal, Indoor and Mobile Radio Communications (PIMRC), Berlin, 2005.

[3] Garcia, A.P. et al.: 60 GHz in-cabin real-time channel sounding, in Fourth Int. Conf. on Communications and Networking in China (ChinaCOM), Xian, 2009.

[4] Garcia, A.P.; Kotterman, W.; Trautwein, U.; Bruckner, D.; Kunisch, J.; Thoma, R.S.: 60 GHz time-variant shadowing characterization within an Airbus 340, in Proc. 4th European Conf. on Antennas and Propagation (EuCAP), Barcelona, 2010.

[5] Singh, H.; Oh, J.; Kweon, C.Y.; Qin, X.; Shao, H.; Ngo, C.: A 60 GHz wireless network for enabling uncompressed video communication. IEEE Commun. Mag., **46** (12) (2008), 71–78.

[6] Wollenschlager, F. et al.: Measurement of a 60 GHz antenna array fed by a planar waveguide-to-microstrip transition integrated in low-temperature co-fired ceramics, in 3rd European Conference on Antennas and Propagation (EuCAP), Berlin, 2009.

[7] Martínez-Vázquez, M.; Oikonomopoulos-Zachos, C.; Maulwurf, K.; Wollenschläger, F.; Stephan, R.; Hein, M.A.; Xia, L.; Müller, J.; Estañ, C.; Dombrowski, K.; Brankovic, V.; Radovic, D.: Highly integrated antennas and front-ends for 60 GHz WLAN Applications, EuMA International Journal of Microwave and Wireless Technologies, Vol. **3**, No. 2, 2011.

[8] Part 11: Wireless LAN medium access control (MAC) and physical layer (PHY) specifications – Amendment 6: enhancements for very high throughput in the 60 GHz band, IEEE P802.11ad/D1, September 2010.

[9] Kmec, M.; Sachs, J.; Peyerl, P.; Rauschenbach, P.; Thomä, R.S.; Zetik, R.: A novel ultra-wideband real-time MIMO channel sounder architecture, in Int. Union of Radio Science (URSI): XXVIII General Assembly, New Delhi, 2005.

[10] Garcia, A.P. et al.: 60 GHz-ultrawideband real-time multi-antenna channel sounding for multi giga-bit/s access, in IEEE 72nd Vehicular Technology Conf. (VTC-Fall), Ottawa, 2010.

[11] Garcia, A.P. et al.: Dual-polarized architecture for ultrawideband channel sounding at 60 GHz with digital/analog phase control based on 0.25 μm SiGe BiCMOS and LTCC technology, in 5th European Conf. on Antennas and Propagation (EuCAP), Rome, 2011.

[12] Kunisch, J.; Pamp, J.: UWB radio channel modeling considerations, in Proc. Int. Conf. Electromagnetics in Adv. Applications (ICEAA), Turin, 2003.

[13] Molisch, A.F. et al.: IEEE 802.15.4a Channel Model –Final Report, IEEE 802.15.4a WPAN Task Group, 2005.

[14] Saleh, A.; Valenzuela, R.: A statistical model for indoor multipath propagation. IEEE J. Sel. Areas Commun, **SAC-5** (2) (1987), 128–137.

[15] Website: http://www.remcom.com/wireless-insite.

[16] Felbecker, R.; Keusgen, W.; Peter, M.: Ray-tracing simulations of the 60 GHz incabin radio channel, in Int. Union of Radio Science (URSI): XXIX General Assembly, Chicago, 2008.

[17] Schulte, B.; Peter, M.; Felbecker, R.; Keusgen, W.; Steffen, R.; Schumacher, H.; Hellfeld, M.; Barghouthi, A.; Ziegler, V.: 60 GHz WLAN Applications and Implemention Aspects, EuMA International Journal of Microwave and Wireless Technologies, Vol. **3**, No. 2, 2011.

[18] Peter, M.; Keusgen, W.; Kortke, A.: Temporal structure of the 60 GHz wireless channel, in 2nd Int. ITG Conf. on Antennas (INICA), Munich, 2007.

[19] Peter, M.; Felbecker, R.; Keusgen, W.; Hillebrand, J.: Measurement-based investigation of 60 GHz broadband transmission for wireless in-car communication, in IEEE 70th Vehicular Technology Conf. (VTC-Fall), Anchorage, 2009.

[20] Krone, S.; Guderian, F.; Fettweis, G.P.; Petri, M.; Piz, M.; Marinkovic, M.; Peter, M.; Felbecker, R.; Keusgen, W.: Physical layer design, link budget analysis and digital baseband implementation for 60 GHz short-range applications, EuMA International Journal of Microwave and Wireless Technologies, Vol. **3**, No. 2, 2011.

[21] Ulusoy, A.C.; Liu, G.; Peter, M.; Felbecker, R.; Abdine, H. Y.; Schumacher, H.: A BPSK/QPSK receiver architecture suitable for low-cost ultra-high rate 60 GHz wireless communications, in European Microwave Conf. (EuMC), Paris, 2010.

Alexis Paolo Garcia Ariza received his M.S. degree in electronic engineering from the Industrial University of Santander (UIS), Bucaramanga, Colombia, in 2002, and Ph.D. in telecommunications from Polytechnic University of Valencia (UPV), Valencia, Spain, in 2009. Since 2008, he is with the Electronic Measurement Research Laboratory (EMT), Ilmenau University of Technology, Ilmenau, Germany. His areas of interest include 60 GHz broadband links, 60 GHz channel sounding, characterization and modeling, and 60 GHz ultra-wideband frontends for polarimetric and directional characterization.

Prof. Dr.-Ing. Reiner S. Thomä received the Dipl.-Ing. (M.S.E.E.), Dr.-Ing. (Ph.D.E.E.) and the Dr.-Ing. habil. degrees in electrical engineering and information technology from Technische Hochschule Ilmenau, Germany, in 1975, 1983, and 1989, respectively. Since 1992, he has been a professor of electrical engineering at TU Ilmenau where he is the head of Electronic Measurement Research Laboratory (EMT). He has contributed to many European and German research projects and clusters. He was awarded IEEE Fellow Member (2007) and received a German Research Award for his contributions to high-resolution multidimensional channel sounding.

Frank Wollenschläger received his Dipl.-Ing. degree in theoretical electrical engineering in 2008 from Technical University of Ilmenau. He joined the RF and Microwave Laboratory at Technical University of Ilmenau in 2008, where his research focuses on modeling and simulation of planar millimetre-wave antennas and their implementation on multilayer ceramics technology.

Robert Müller received his M.S. degree in electronic engineering from the Berlin University of Technology (TUB), Germany, in 2009. Since 2009, he is Ph.D. student with the Electronic Measurement Research Laboratory (EMT), Ilmenau University of Technology, Germany. His areas of interest include high-frequency components and system designs. He also developed investigations in 60 GHz broadband links and 60 GHz channel sounding.

Uwe Trautwein received his Dipl.-Ing. degree in electrical engineering in 1993 from Technical University of Ilmenau and worked for several years at the same institution. He worked as a visiting researcher at Vienna University of Technology, Austria, and with the NTT DoCoMo Wireless Laboratory at YRP, Yokosuka, Japan. Since 2001 he is with the company MEDAV in Ilmenau where he is responsible for system design and test of radio measurement equipment such as direction finders.

Itziar de la Torre received her Ingeniero Superior de Telecomunicaciones degree from the University of the Basque Country (UPV/EHU), Bilbao, Spain, in 2005. She is currently working at the Information and Communication Systems department of IMST GmbH, Kamp-Lintfort, Germany. Her main research interests include analysis of wave propagation, ray-tracing simulations, radar signal processing, and indoor localization systems.

Jürgen Kunisch obtained the Dipl.-Ing. and Dr.-Ing. degrees in electrical engineering from the University of Duisburg, Germany, in 1989 and 1994. Currently, he is the head of the wave propagation and radar methods section of IMST GmbH in Kamp-Lintfort, Germany. His working areas include radar signal processing, the physical layer of mobile communication and localization systems, and in particular measuring and modeling of radio wave propagation.

Michael Peter received his diploma degree in electrical engineering and information technology from the University of Karlsruhe, Germany, in 2004. In 2005 he joined the Fraunhofer Heinrich Hertz Institute in Berlin. His research activities focus on 60 GHz communication, wideband channel modeling, and physical layer design of wireless broadband communication systems.

Robert Felbecker received his Dipl.-Ing. (M.S.E.E.) degree from the RWTH Aachen University, Germany, in 2007. Since 2007 he is with the Fraunhofer Heinrich Hertz Institute in Berlin, Germany. He is involved in the fields of measurement and simulation of electromagnetic wave propagation.

Wilhelm Keusgen received the Dipl.-Ing. (M.S.E.E.) and Dr.-Ing. (Ph.D.E.E.) degrees from the RWTH Aachen University, Aachen, Germany, in 1999 and 2005, respectively. From 1999 to 2004, he was with the Institute of High Frequency Technology, RWTH Aachen University. In 2004 he has joined the Fraunhofer Heinrich Hertz Institute, Berlin. His main research areas are millimeter-wave communication, car-to-car communication, and digital compensation of RF impairments especially for power amplifiers.

https://doi.org/10.1017/S1759078711000092 Published online by Cambridge University Press